when the carbon atoms are situated at the equilibrium sites (Table 1). A B_{ij} value near 20·0 Å^2 implies an r.m.s. amplitude of vibration of about 0·5 Å which would be similar to a displacement of 0·16 Å off the axis (to relieve crowding) and a B_{ij} value near 7·0 Å^2. Further evidence that the large thermal parameters for the carbon atoms result from disordering rather than from large thermal motion may be obtained by noting any decrease in thermal diffuse scattering when the crystals are cooled. However, no change was noted in diffraction photographs when the crystals were cooled to 77°K. In addition, if the large thermal parameters were due to thermal motion, a phase change might occur upon cooling as this motion is restricted or frozen into the lowest energy state (unless this would result in statistical ordering). However, no phase change is observed by diffraction to 77°K or by changes in the electron absorption spectra to 5°K (Lawson, 1967). This suggests that the interpretation that the high carbon thermal parameters result from the statistical and positional disordering of the $[N(CH_3)_4]^+$ ion is correct.

The assistance of R. A. Trudo is gratefully acknowledged.

References

International Tables for X-ray Crystallography (1962). Vol. III, Birmingham: Kynoch Press.

LAWSON, K. (1967). *J. Chem. Phys.* To be published.

MOROSIN, B. & GRAEBER, E. J. (1965). *J. Chem. Phys.* **42**, 898.

MOROSIN, B. & LINGAFELTER, E. C. (1959). *Acta Cryst.* **12**, 611.

PAULING, L. (1960). *The Nature of the Chemical Bond.* 3rd ed. Ithaca: Cornell Univ. Press.

STUCKY, G., D'AGOSTINO, S. & MCPHERSON, G. (1966). *J. Amer. Chem. Soc.* **88**, 4828.

WIESNER, J. R., SRIVASTAVA, R. C., KENNARD, C. H. L., DIVAIRA, M. & LINGAFELTER, E. C. (1967). *Acta Cryst.* To be published.

WILLETT, R. D. (1966). *J. Chem. Phys.* **45**, 3737.

Acta Cryst. (1967). **23**, 770

The Structure of Molybdenum Pentachloride-Graphite by Single-Crystal Electron and X-ray Diffraction*

BY A. W. SYME JOHNSON†

C.S.I.R.O. Division of Chemical Physics, Chemical Research Laboratories, Melbourne, Australia and Physics Department, University of Western Australia, Nedlands, Western Australia

(*Received* 19 *December* 1966)

The structures found in the 4th stage graphite lamellar compound containing 24·8 % $MoCl_5$ have been determined by a combination of single-crystal electron-diffraction and X-ray-diffraction methods. The use of the latter technique showed sets of four adjacent graphite sheets to retain the normal *ABAB* stacking and interlayer spacing of free graphite. Electron diffraction showed the lateral structure within each graphite sheet to be unchanged and the intercalated molybdenum pentachloride layers to exist in two or more phases. In the most clearly characterized of these phases the dimer molecular structure of the free pentachloride is preserved, the molecules lying in a close-packed array having a precise orientation to the adjacent graphite sheets. The measurable intramolecular atomic distances of the dimer molecule remain unchanged from those in the free chloride but owing to interaction with the graphite the molecular symmetry is lower than that possessed by non-intercalated molecules. The other reactant layer phases are characterized by hexagonal and disordered cation distributions, the dimeric relationship no longer being distinguishable. A substructure consisting of two adjacent pseudo close-packed chlorine layers is common to all phases, individual phases being distinguished by the cation distribution within the octahedral sites. Certain orientations of the substructure relative to the graphite are more highly favoured, the reactant at other orientations being characterized by a disordered cation distribution and an increase in the mean chlorine–chlorine distance measured parallel to the layer plane.

Introduction

Generally the mechanism of formation of a lamellar graphite compound, that is the penetration of a graphite crystal at many independent points on its prismatic faces by the reactant atoms or molecules, automatically results in a disordered and multiply twinned condition of the intercalated crystal. Consequently structural knowledge of these compounds is difficult to obtain by single-crystal X-ray methods. The greater resolving power of microbeam electron diffraction and its ability to select minute ordered regions of the crystal avoids

* This work formed part of a thesis for the degree of Doctor of Philosophy submitted in the University of Western Australia.

† Permanent address: CSIRO, Division of Chemical Physics, P.O. Box 160, Clayton, Victoria, Australia.

the difficulties of interpreting the X-ray patterns and allows a projection of the structure normal to the layer plane to be derived from electron diffraction intensities (Cowley & Ibers, 1956). A rational interpretation of the X-ray patterns on the basis of the electron diffraction projection data is then feasible leading in favourable circumstances to a three-dimensional structure. Despite this opportunity the structures of most known lamellar graphite compounds, apart from bromine–graphite (Eeles & Turnbull, 1965) and $FeCl_3$–graphite (Cowley & Ibers, 1956), are unknown (see Croft, 1960; Hennig, 1959; Rüdorff, 1959; Rüdorff, Stumpp, Spriessler & Siecke, 1963).

In general the lamellar graphite compounds are ideally suited for structural investigation by single-crystal electron diffraction since the conditions for kinematic scattering are well satisfied. This is a consequence of a lack of lateral coherence between the reactant layers and their host graphite crystal, a condition found to exist in the compound studied in the present work. As a result, a kinematic approximation proved adequate for the interpretation of structural data.

Preparation and properties

The compound was prepared by Croft (1956*a*) by heating at 300 °C purified graphite (60 to 100 mesh, ash content 0·02%) and an excess of anhydrous $MoCl_5$ in an atmosphere of nitrogen. Flotation of the resulting black, brittle crystals in bromoform–chloroform mixtures indicated a wide density variation. This was consistent with the incomplete state of intercalation demonstrated later by electron microscope and diffraction experiments. Chemical analysis gave the average composition as 24·8% $MoCl_5$, considerably lower than the theoretical composition of 35·5% for a stage 4 compound (4 graphite sheets per reactant layer) derived from diffraction data.

The structure of molybdenum pentachloride

Solid molybdenum pentachloride adopts the dimeric molecular structure of $NbCl_5$ and $TaCl_5$ in which two cations occupy adjacent octahedral sites formed by the superposition of two quasi close-packed anion layers containing five chlorine atoms each (Sands & Zalkin, 1959). Close packing of these molecules leads to a crystal structure with the following cell constants:

Monoclinic, $C2/m$ (b axis unique)
12 $MoCl_5$ units per cell
$a = 17{\cdot}31 \pm 0{\cdot}01$ Å
$b = 17{\cdot}81 \pm 0{\cdot}01$
$c = 6{\cdot}079 \pm 0{\cdot}005$
$\beta = 95{\cdot}7° \pm 0{\cdot}1°$
$\varrho_{cal} = 2{\cdot}936$ g.cm^{-3} .

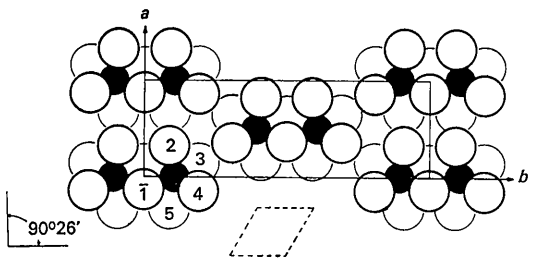

Fig. 2. The molecular arrangement in $MoCl_5$ reactant layers of the dimer phase. Solid lines define the unit cell. The subcell containing two chlorine atoms (open circles) and one octahedral site is depicted by dotted lines.

Electron diffraction observations

Thin flakes of $MoCl_5$–graphite were prepared for electron diffraction by wiping a single crystal across a specimen grid previously treated with pressure-sensitive adhesive. Selected-area diffraction patterns and dark-field images were recorded from crystal regions approximately 2 microns square in Hitachi HU 11A and JEM 6A electron microscopes operating at 75 and 80 keV respectively.

The interpretation of typical $hk0$ electron diffraction patterns such as that shown in Fig. 1 was complicated by simultaneous diffraction from two main reactant layer phases. One had an oblique two-dimensional unit cell and so six equivalent but distinguishable orientations with respect to the host crystal, the other a hexagonal two-dimensional unit cell in two distinguishable orientations. Generally the patterns from both of these phases were observed along with the $hk0$ graphite pattern which forms the intense hexagonal array of Fig. 1. The latter was used for a standard spacing in all diffraction pattern measurements since X-ray comparison of single crystals against a silicon powder standard* showed no change in the graphite a-axis dimension on intercalation.

A consideration of both the packing of Mo_2Cl_{10} groups in the space available to a reactant layer and the bulk unit-cell dimensions given above suggested a structure with an orthogonal centred cell of plane group symmetry *cmm* and approximate axes of $a = 6{\cdot}1$, $b = 17{\cdot}8$ Å (Fig. 2). The sixfold oriented phase mentioned above, subsequently referred to as the dimer phase, supported this suggestion, an approximately orthogonal ($\gamma = 90°26'$) centred unit cell with axes $a = 6{\cdot}09 \pm 0{\cdot}01$ and $b = 17{\cdot}79 \pm 0{\cdot}04$ Å measured relative to graphite (100) of 2·131 Å being observed in an orientation such that an exact fit of the graphite (100) and $MoCl_5$ ($2\bar{6}0$) planes could occur. As the plane symmetry was $p2$ a conventional primitive unit cell should have been chosen. However the centred cell was preferred as it emphasized the symmetry variations resulting from intercalation, facilitating comparison of the intercalated and free structures.

The diffraction patterns of the dimer phase were characterized by strong $0,10$; $3,5$ and $3,\bar{5}$ reflexions, resulting from a two-layer close-packed chlorine sub-

* The Si standard sample was taken from that supplied for the I.U.Cr. Lattice Parameter Project (Parrish, 1960).

structure. The same substructure at a different orientation to the graphite was also observed in the hexagonal phase, strong 3,0 reflexions linked by diffuse arcs to the *0,10*; *3,5* and *3,$\bar{5}$* reflexions of the dimer phase being present in the diffraction patterns (see Fig. 1). Thus both dimer and hexagonal reactant layer phases could be assumed to possess a similar structure, that of two close-packed chlorine layers sandwiched together but differing in the cation occupation of octahedral sites. The difference between the angular relations of the dimer and hexagonal phases with graphite is shown in Fig. 3. The hexagonal phase was found to have a unit-cell edge of $6{\cdot}182 \pm 0{\cdot}01$ Å and to be oriented with its plane at an angle of $33°42' \pm 5'$ to the graphite (100)(100).

The apparent dependence of the orientation of reactant layers on cation configuration suggested that a measurement of atomic parameters in projection might lead to a better understanding of the epitaxic forces acting within the compound. Accordingly a structural investigation of the dimer phase was undertaken.

The structure of the dimer phase

Single-crystal selected-area electron diffraction patterns were used for the visual estimation of reactant layer *hk*0 relative intensities. A geometric series of timed exposures at 2, 4, 8 up to 64 seconds allowed at least four independent measurements of each reflexion to be made. Drift in intensity was measured by making further exposures of 2 and 4 seconds. To avoid errors resulting from objective lens malfocusing and spherical aberration (Reiche, 1961), areas of at least 4 μ^2 were selected from crystal regions whose $MoCl_5$ dark-field images showed no contrast within considerably larger areas of approximately 9 μ^2. Correct objective focusing was ensured by obtaining the same crystal regions in centrosymmetrically related dark-field images formed by a slight defocusing of the intermediate lens from the diffraction pattern setting. The reliability of these procedures was checked later by comparing the measured intensities of reflexions and their inversions. Equality in this comparison was a criterion for the selection of patterns for intensity measurement.

Since the structure of the dimer reactant layer phase was virtually determined by the pseudo-hexagonal chlorine sublattice, the set of reflexions of one orientation whose indices could be expressed as

$$h, 5h+10n \text{ where } n=0, \pm 1, \pm 2 \ldots$$

partially overlapped similar sets from orientations at 60 and 120° to the first. Provided the amount of reactant in the three orientations differed, the contributions of each to the intensity of a particular reflexion in the set could be calculated from an associated group of three linear simultaneous equations. The observed amplitudes E_o bracketed in Table 1 are the results of such calculations.

The strong graphite reflexions offered a means of checking for the presence of secondary elastic scattering, intensity measurements being made only on patterns in which this effect was negligible.

Refinement

During refinement a centre of symmetry was assumed and no account was taken of possible contributions to the reactant layer diffraction pattern from carbon atoms. The $2,\bar{6},0$ and $4,\bar{12},0$ reflexions were omitted because of their coincidence with the graphite 100 and 200.

Table 1. *Observed and calculated electron diffraction structure amplitudes (volts) for the dimer reactant layer phase*

( ) denotes overlapped reflexions, see text.
* and — denote reflexions of the form $h,\bar{3}h,0$.

H	K	L	$10E_o$	$10E_c$	H	K	L	$10E_o$	$10E_c$
0	2	0	8.76	7.78	3	-15	0	(5.24)	(-5.01)
0	4	0	18.31	-18.62	3	17	0	< 1.19	-0.85
0	6	0	6.59	-6.75	3	-17	0	< 1.19	-0.33
0	8	0	2.75	2.09	3	19	0	< 1.19	.62
0	10	0	(20.03)	(27.01)	3	-19	0	1.30	.85
0	12	0	2.11	2.77	3	21	0	< 1.19	-0.31
0	14	0	4.16	-3.60	3	-21	0	< 1.19	-0.46
0	16	0	< 1.19	.93	4	0	0	(1.73)	(-4.75)
0	18	0	< 1.19	.44	4	2	0	1.73	2.17
0	20	0	(2.16)	(2.64)	4	-2	0	2.11	1.91
0	22	0	< 1.19	.41	4	4	0	6.75	-6.55
1	1	0	21.44	21.35	4	-4	0	8.53	-8.27
1	-1	0	21.44	21.15	4	6	0	5.40	-6.23
1	3	0	10.58	-11.21	4	-6	0	6.10	-6.87
1	-3	0	11.66*	-12.53	4	8	0	2.81	3.14
1	5	0	(7.99)	(10.37)	4	-8	0	3.78	3.95
1	-5	0	(5.72)	(7.62)	4	10	0	(1.40)	(-2.88)
1	7	0	2.54	2.71	4	-10	0	(2.27)	(-1.66)
1	-7	0	1.78	1.86	4	12	0	1.08	-1.16
1	9	0	7.61	7.67	4	-12	0	- *g*	-
1	-9	0	8.91	10.12	4	14	0	1.62	-1.48
1	11	0	3.94	3.73	4	-14	0	3.19	-2.46
1	-11	0	4.75	5.96	4	16	0	< 1.19	-1.25
1	13	0	4.59	-4.83	4	-16	0	1.67	-1.67
1	-13	0	4.05	-4.74	4	18	0	< 1.19	.80
1	15	0	(2.21)	(2.26)	4	-18	0	< 1.19	1.04
1	-15	0	(2.21)	(1.24)	4	20	0	(<1.19)	(-0.60)
1	17	0	2.38	2.14	4	-20	0	(<1.19)	(-0.37)
1	-17	0	1.40	1.63	5	1	0	< 1.19	-0.58
1	19	0	1.30	1.04	5	-1	0	1.89	-1.23
1	-19	0	1.94	1.36	5	3	0	< 1.19	.47
1	21	0	< 1.19	.22	5	-3	0	.92	-0.97
1	-21	0	< 1.19	.64	5	5	0	(1.30)	(-2.01)
2	0	0	(6.10)	(.33)	5	-5	0	(1.62)	(-2.36)
2	2	0	< 1.19	.34	5	7	0	< 1.19	.74
2	-2	0	< 1.19	-1.89	5	-7	0	1.89	1.85
2	4	0	6.21	-6.05	5	9	0	< 1.19	.25
2	-4	0	7.07	-6.82	5	-9	0	1.40	1.04
2	6	0	2.75	-2.22	5	11	0	< 1.19	-1.09
2	-6	0	- *g*	-	5	-11	0	1.62	-1.49
2	8	0	4.54	4.10	5	13	0	< 1.19	-0.35
2	-8	0	6.59	6.15	5	-13	0	1.94	-1.34
2	10	0	(3.40)	(.03)	5	15	0	(<1.19)	(-0.46)
2	-10	0	(4.81)	(-0.42)	5	-15	0	(<1.19)	(-0.71)
2	12	0	2.43	-2.40	5	17	0	< 1.19	.33
2	-12	0	4.10	-3.92	5	-17	0	1.40	.83
2	14	0	1.94	-2.12	6	0	0	(4.64)	(4.36)
2	-14	0	2.21	-2.48	6	2	0	< 1.19	.95
2	16	0	< 1.19	-0.02	6	-2	0	< 1.19	.86
2	-16	0	1.40	.95	6	4	0	1.51	-1.63
2	18	0	1.30	1.05	6	-4	0	1.62	-1.73
2	-18	0	2.21	1.88	6	6	0	< 1.19	-1.02
2	20	0	(1.19)	-0.07	6	-6	0	.92	-1.08
2	-20	0	(1.19)	-0.11	6	8	0	< 1.19	.68
2	22	0	< 1.19	-0.51	6	-8	0	1.51	.95
2	-22	0	< 1.19	-0.88	6	10	0	(2.70)	(2.20)
3	1	0	6.10	7.07	6	-10	0	(3.02)	(2.30)
3	-1	0	6.10	7.79	6	12	0	< 1.19	.44
3	3	0	2.97	-3.19	6	-12	0	< 1.19	.09
3	-3	0	3.13	-3.13	0	0	0	-	89.17
3	5	0	(19.06)	(-25.71)					
3	-5	0	(25.33)	(-25.99)					
3	7	0	2.65	-3.06					
3	-7	0	2.75	-2.59					
3	9	0	4.64	4.76					
3	-9	0	5.40*	5.00					
3	11	0	1.08	.61					
3	-11	0	1.08	.57					
3	13	0	< 1.19	-0.72					
3	-13	0	1.62	-1.24					
3	15	0	(4.21)	(-4.92)					

Structure factors, E_c,* were calculated for the centred unit cell of the dimer phase described earlier ($a=6{\cdot}09$, $b=17{\cdot}79$, $\gamma=90°26'$) but using the molecular dimensions given by Sands & Zalkin (1959). These were compared with scaled values of the observed amplitudes E_o. The discrepancy index R, calculated omitting unobserved reflexions for which E_c was less than the minimum observable value of E_o, was 24%. Difference Fourier refinement would not reduce R to less than 20%, strong spurious peaks not connected in any obvious way to the structure being refined persisting in the difference Fourier maps. Agreement between the observed and calculated data was significantly poorer for the reflexions of the set, $h, 5h+10n, n=0, \pm1, \pm2$, *etc.* Without them R dropped to 17%. Since these reflexions relate to the structural unit containing two chlorine atoms and one octahedral site (dotted in Fig. 2) they will contain contributions from regions of the crystal where either imperfect packing of the dimer molecules has occurred resulting from their orientation at 60° or 120° to the remainder of the reactant in the same layer, or where cation disorder exists. The procedure for dissecting the intensity contributions from differing orientations would be invalidated if the proportion of disordered or imperfectly packed reactant varied with orientation, since the contributing ratios for the three orientations are calculated from reflexions due only to ordered molecules. Consequently, the reflexions $h, 5h+10n$ were omitted in the later refinement which gave a discrepancy index of 9·5% and the difference Fourier and Fourier maps† shown in Fig. 4. The corresponding structure amplitudes, atom parameters and interatomic distances are given in Tables 1, 2 and 3.

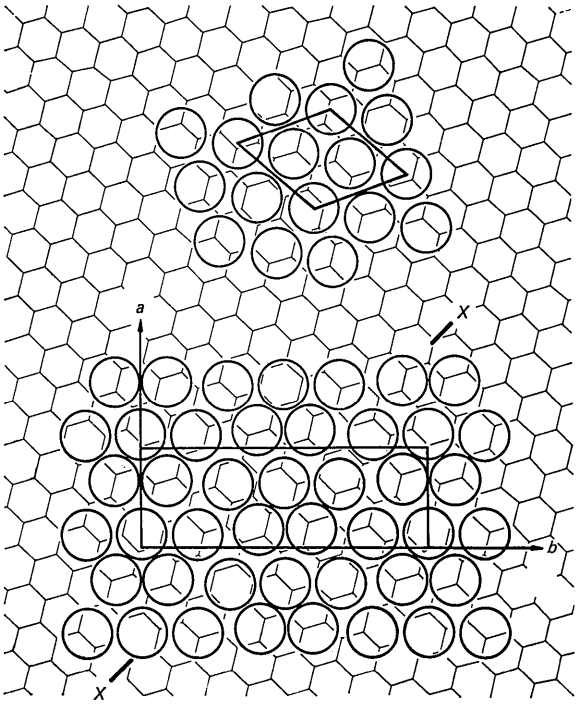

Fig. 3. The angular arrangement of the graphite lattice (fine lines) with respect to the nearest chlorine atoms (circles) of reactant layers. Upper group: the 3·7° hexagonal phase. Lower group: the dimer phase, X–X being parallel to the set of graphite (100) planes operating in aligning the reactant orientation shown. The graphite net is shown only to indicate the orientation and scale of the structures and does not imply knowledge of the relative positions of carbon and chlorine atoms.

* A relativistic correction was applied for wavelength only, not for mass (Fujiwara, 1961; Goodman & Lehmpfuhl, 1967). Atomic scattering curves were taken from tables given by Dawson (1961) for un-ionized chlorine and from *International Tables for X-ray Crystallography* (1962) for un-ionized molybdenum.

† The Fourier map of Fig. 4 was calculated with the use of E_c for the reflexions h, $5h+10n$.

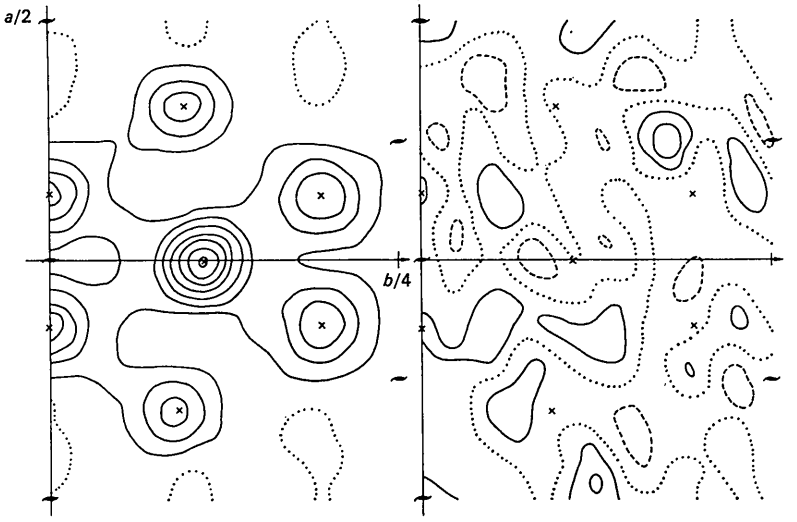

Fig. 4. Fourier and difference Fourier projected potential maps for the dimer phase of $MoCl_5$ in graphite. Contour interval of Fourier map, 5 volt.Å, of difference Fourier map, 0·5 volt.Å; projected distance, 6·14 Å. Zero contour, dotted lines; negative contours, dashed lines. Crosses mark the atomic positions given in Table 2.

Table 2. *Atomic parameters in intercalated* $MoCl_5$ *deduced from electron diffraction data*

	x	y	B (Å²)	
Mo	−0·003 (0·0)*	0·108 (0·1080)	Anisotropic, ⊥ (1$\bar{3}$0) planes B=4·1 ∥ (1$\bar{3}$0) planes B=5·9 (2·2)	
Cl(1)	0·1395 (0·133)	0·0005 (0·0)	3·7	(2·8)
Cl(2)	0·323 (0·323)	0·0969 (0·094)	4·8	(3·1)
Cl(3)	0·1343 (0·145)	0·194 (0·192)	4·7	(4·3)
Cl(4)	−0·137 (−0·145)	0·194 (0·192)	4·7	(4·3)
Cl(5)	−0·315 (−0·323)	0·0916 (0·094)	5·2	(3·1)

* The parameters in brackets are those found by Sands & Zalkin (1959) for the free molecules, recalculated so as to refer to the unit-cell axes of the intercalated structure.

Table 3. *Some nearest neighbour distances in intercalated and free molybdenum pentachloride*

Atom pair	z*	Distance Intercalated	Free
Mo—Mo	0·0 Å	3·84±0·01 Å	3·84±0·02 Å
Cl($\bar{1}$)–Cl(2)	+1·37	3·30±0·03	3·24±0·03
Cl(1)–Cl(5)	−1·37	3·21±0·04	3·24±0·03
Cl(2)–Cl(4)	+1·37	3·30±0·03	3·29±0·03
Cl(3)–Cl(5)	−1·37	3·28±0·04	3·29±0·03
Cl($\bar{1}$)–Cl(4)	+1·37	3·46±0·03	3·41±0·03
Cl(1)–Cl(3)	−1·37	3·44±0·03	3·41±0·03
Cl(2)–Cl($\bar{5}$)	+1·37	3·36±0·04	3·34±0·04

* Mean coordinate of the layer containing both atoms.

A comparison of some interatomic distances in free molybdenum pentachloride (Sands & Zalkin, 1959) with those of the graphitically intercalated molecule (Table 3) shows no significant differences resulting from lamellar compound formation. The main effect is a distortion in the packing of the molecules resulting from their exact location on a graphite (100) plane as depicted for one of the six equivalent reactant orientations in Fig. 5. Evidence for this location is the precise fit and sharpness of the graphite $h00$ and $MoCl_5$ $2h,\bar{6}h,0$ reflexions and the diffuseness of the $MoCl_5$ reflexions which increases with their perpendicular distance from the $[1,\bar{3},0]$* direction. It is important to note that if the graphite had not influenced the packing of the reactant molecules their natural *mmm* symmetry would have resulted in a rectangular unit cell. Direct evidence of the distortion provided by dark-field Moiré fringes will be described in a later section of this paper.

The structures of the hexagonal phases

The hexagonal reactant layer phase discussed earlier was the most frequently observed of three such phases listed in Table 4. The name of each phase was derived from the angle between its a axis and that of the graphite, less 30°. In Fig. 6 electron diffraction patterns from the three phases appear simultaneously, each in two-fold orientation, together with spots from other unindexed but much less favoured phases.

A decisive clue to the structure of the prominent 3·7° phase was provided by the similarity of its diffraction patterns to those of graphitically intercalated

Table 4. *Data for the hexagonal phases of molybdenum chloride in graphite*

Name	Frequency of observation*	a_{hex}	Angle between a axis and $a_{graphite}$
0°	1 %	6·195±10 Å	30°
3·7	75	6·182±10	33°42′±5′
6·1	1	6·160±10	36 4 ±6

* By electron diffraction; the dimer phase accounted for the remainder of the observations.

ferric chloride (Cowley & Ibers, 1956). The structure of a ferric chloride layer is characterized in diffraction by strong 300 and 100 reflexions, the former decreasing in intensity as the crystal is tilted away from normal incidence, coupled with weak 110 and 220 reflexions whose intensities increase upon tilting. The 3·7° phase $hk0$ diffraction pattern demonstrated these general properties and in particular reflexions of the form $h-k\neq 3n$, $n=0,1,2\ldots$ (arrowed in Fig. 6) varied from intense and sharp to weak and diffuse in character. This may be interpreted by assuming the undistorted

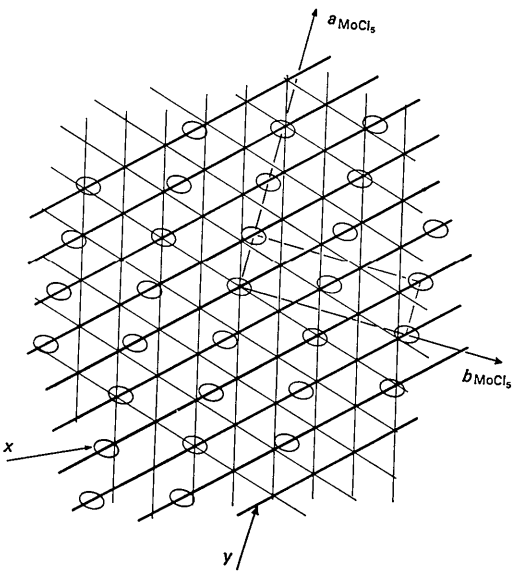

Fig. 5. A diagrammatic view of the dimer molecules, X, of one orientation in relation to the three equivalent sets of graphite (100) planes. The set Y is that operating in aligning the reactant orientation shown. Only every second (100) plane has been drawn.

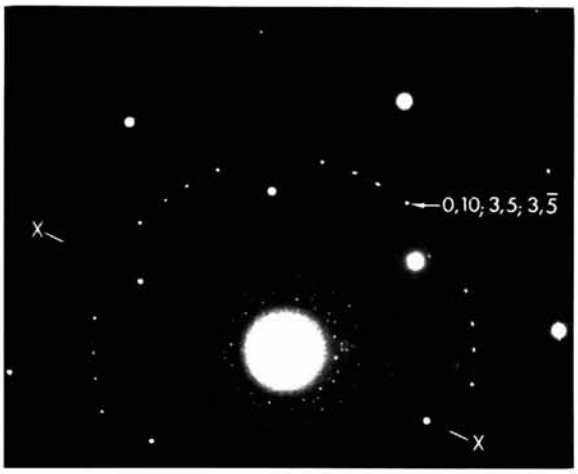

Fig. 1. Single-crystal electron diffraction pattern from $MoCl_5$–graphite. The strong widely spaced spots are the graphite $hk0$ reflexions, the remainder $hk0$ reflexions from dimer and 3·7° hexagonal phases of $MoCl_5$.

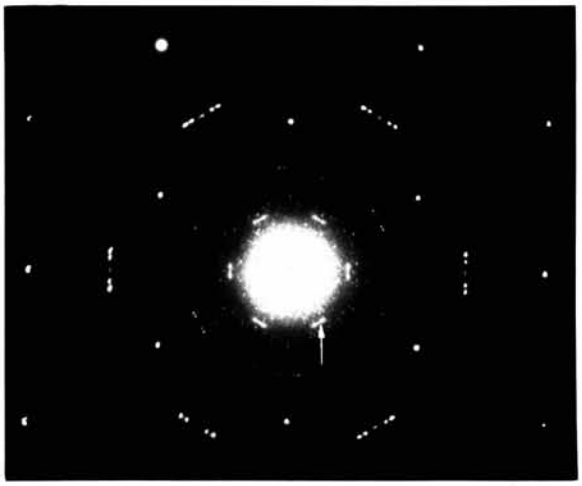

Fig. 6. Electron diffraction pattern from an intercalated crystal in which three hexagonal molybdenum chloride phases co-exist. The rows of five strong spots are their 300 reflexions and the varied diffuse character of the 100 spots is clearly apparent (arrowed).

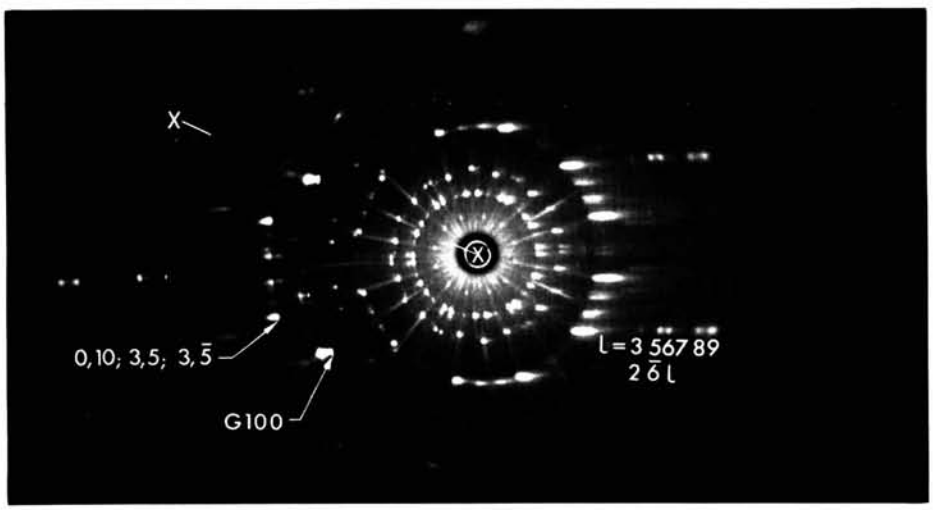

Fig. 7. Oscillation photograph of 24·8 % $MoCl_5$–graphite confirming the dimer phase deduced from electron diffraction evidence to be characteristic of bulk crystals (*cf.* Fig. 1). Cu $K\alpha$ radiation.

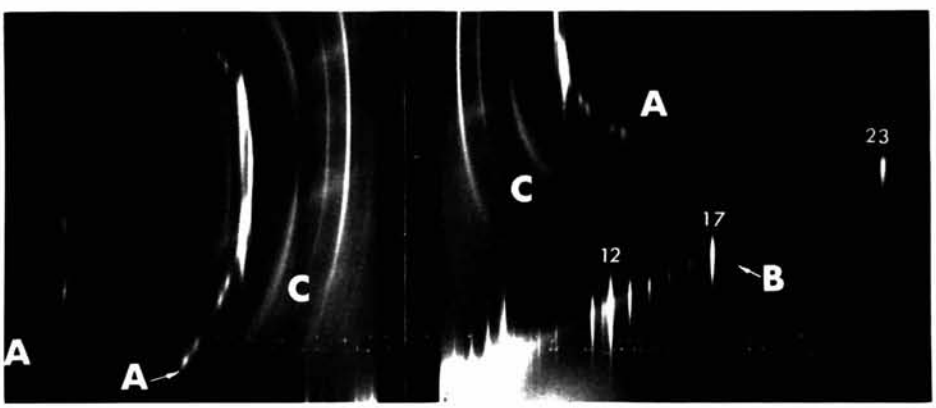

Fig. 8. Weissenberg photograph of 24·8 % $MoCl_5$–graphite showing a section through reciprocal space containing the c axis and the line $X-X$ in Figs. 1 and 7. *A*, the $2h\ \bar{6}h\ l$ reflexions; *B*, the strong arced $00l$ reflexions; *C*, the continuous streak of the $1\bar{3}0$ reflexions. Some faint extra lines in the low-angle region of the set *B* are due to X-ray tube impurities. Cu $K\alpha$ radiation.

[*To face p.* 774

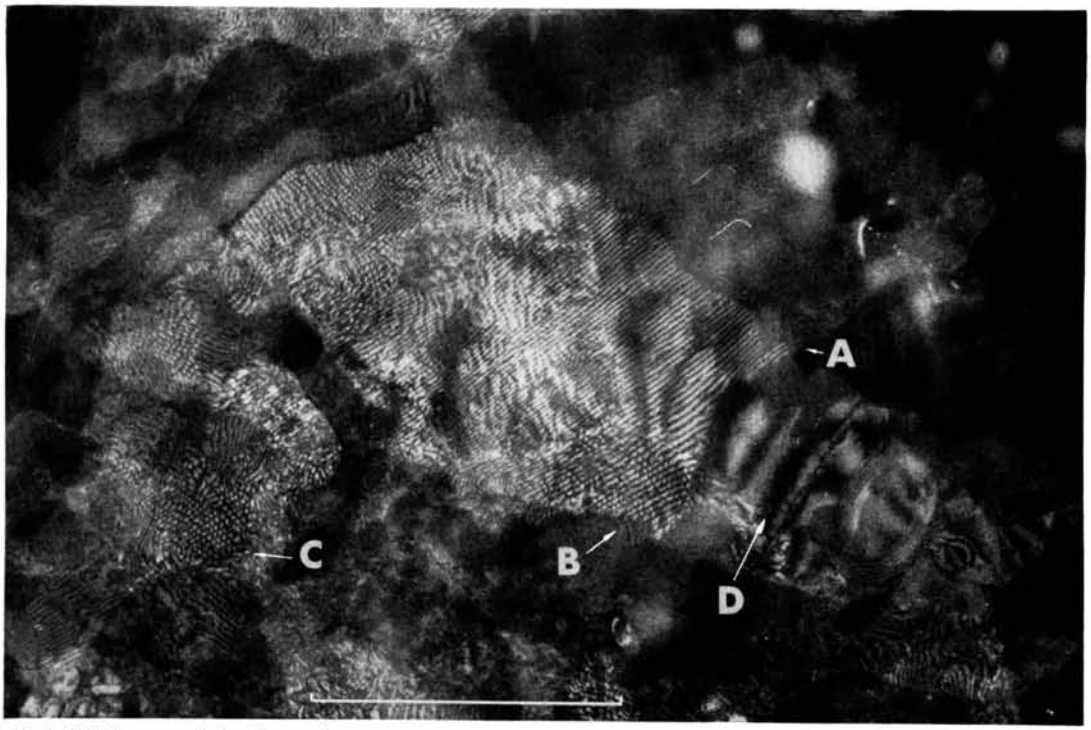

Fig. 12. A dark-field image of the dimer phase reactant showing distorted Moiré fringes where two layers of different orientation overlap. See text for details. The bar indicates one micron.

Fig. 13. The same region at the same magnification as in Fig. 12 but observed with a graphite (100) reflexion.

close-packed chlorine structure and a unit cell such that the octahedral sites are at 0,0; $\frac{1}{3},\frac{2}{3}$ and $\frac{2}{3},\frac{1}{3}$ with occupancies of p, q and r respectively. The reflexions of the form $h-k\neq 3n$, $n=0,1,2\ldots$ receive contributions solely from atoms in octahedral sites and have an amplitude in the centrosymmetric case of $q=r$ given by $E_c=(p-q)g_{Mo}$, where g is the electron diffraction atomic scattering factor. Thus an equal distribution of molybdenum atoms over the three sites would result in a disappearance of the reflexions, whereas hexagonal ordering with every third site occupied ($p=1$, $q=r=0$; $MoCl_6$) or with two out of three occupied ($p=0$, $q=r=1$, $MoCl_3$), would result in the reflexions attaining maximum intensity. The expressions for the structure amplitudes for the remaining reflexions,

$$E_c=-3g_{Cl}+(p+2q)g_{Mo} \text{ when } h-k=3n,\ h\neq 3n$$

and

$$E_c=6g_{Cl}+(p+2q)g_{Mo} \text{ where } h-k=3n,\ h=3n$$

show them to be insensitive to varying cation distributions.

An attempt to obtain quantitative agreement between experimental amplitudes and values calculated* from the foregoing model met with limited success only, the discrepancy index being 65% for a fully ordered $MoCl_3$ stoichiometry and 37% for $MoCl_6$ stoichiometry. Agreement in the latter case improved to 20% when reflexions of the set $h-k=3n$, $h\neq 3n$ were omitted but no obvious changes in occupancy factors or atomic parameters could have been deduced without recourse to Fourier techniques. Because of this conclusion and recent chemical evidence showing that the conditions of preparation of the compound had favoured the production of free chlorine, $MoCl_5$ monomer and $MoCl_4$ (Saeki & Matsuzaki, 1965) as well as $MoOCl_4$ (Colton & Tomkins, 1964), further investigation was curtailed pending the availability of homogeneous specimens of known composition.

X-ray diffraction observations

The X-ray study of the compound had two aims; to establish the layer sequence by reference to the 00*l* reflexions and, by reference to selected *hkl* reflexions to attempt a determination of the relative lateral positions of the dimer reactant phase and graphite. In the dimer case the precise one-dimensional fit of reactant and graphite demonstrated by electron diffraction suggested that a definite site for the reactant molecules might be observed when the structure was viewed in projection along the graphite [010] direction.

*hk*0 *reflexions*

A $\pm 7{\cdot}5°$ oscillation photograph (Fig. 7) taken about the graphite [$\bar{1}$10] with a beam of filtered Cu $K\alpha$ radiation almost normal to the layer plane demonstrates features very similar to those in the patterns of Fig. 1. This confirms that phases found by electron diffraction are characteristic of bulk crystals. The relative strengths of the dimer and 3·7° hexagonal phase patterns show that the former phase accounts for approximately 90% of the reactant in bulk crystals. The infrequent electron diffraction observation of the dimer phase can be ascribed to the automatic selection of crystal edges during preparation or examination of the specimens. The likelihood of intercalation proceeding *via* the monomer, known to exist in the vapour phase of $MoCl_5$ (Bader & Westland, 1961), might favour the presence of hexagonal phases at the edges of an intercalating graphite crystal, association of adjacent cation pairs to form dimers occurring during diffusion of the reactant toward the centre of its host crystal.

The streaking of the reactant reflexions on the right of Fig. 7 results from a lack of diffraction coherence between successive reactant layers. Each therefore diffracts independently as a single layer giving rise to a continuous transform normal to the layer. This is also clearly apparent in Fig. 8 and completely justifies the use of kinematic theory for the interpretation of electron diffraction intensities.

00*l* *reflexions*

The highly regular spacing of the reactant layers suggested that an accurate measurement of the interlayer distances could be obtained from the 00*l* reflexions. It is of fundamental interest to observe in the higher stage lamellar compounds, *i.e.* those in which two or more carbon layers separate adjacent reactant layers, whether intercalation increases or decreases the carbon–carbon interlayer distance relative to that of free graphite (Ubbelohde & Lewis, 1960). No change was observed for $MoCl_5$–graphite.

Strong and sharp reflexions were obtained in single-crystal oscillation and Weissenberg photographs taken with Cu $K\alpha$ and Mo $K\alpha$ radiation using cameras of 5·73 and 8·1 cm diameter respectively. The roughly rectangular crystals *A*, of dimensions 8·0 μ (*c* axis), 145 μ and 450 μ and *B*, of dimensions 96 μ (*c* axis), 320 μ and 610 μ, were both slightly bent, resulting in the extension of the 00*l* reflexions apparent in Fig. 8. In each case the smallest dimension of the crystal was perpendicular to its axis of rotation with the longest dimension parallel to this axis. The repeat distance along the *c* axis of both crystals was found by comparison against silicon powder ($a_0=5{\cdot}4305\pm 5$ Å) to be $19{\cdot}370\pm 5$ Å. Similarly the repeat distance of the virgin graphite was $6{\cdot}710\pm 2$ Å. Intensities were measured by microphotometering across the reflexions, perpendicular to the direction of extension, using a slit length considerably smaller than the length of extension. Because of the nature of the reflexions powder Lorentz factors were applied. Corrections for absorption were significant only for the case of crystal *A* and Cu radiation and were calculated on an IBM 1620 computer with a program due to B. M. Craven. After correcting

* A thermal parameter of 6 Å^2 was deduced by inspection and applied to all atoms in the calculation of structure amplitudes.

for polarization the two resulting sets of observed structure amplitudes F_o, given in Table 5, were used in separate one-dimensional Fourier refinements of the interlayer distances.

00l refinement

A consideration of the structures of intercalated $MoCl_5$ layers and of free graphite together with the *c*-axis repeat distance of 19·37 Å led to a trial arrangement of four graphite layers per reactant layer, confirmed by subsequent agreement of calculated and observed structure amplitudes. The calculated amplitudes were obtained with the use of the form factors for unionized Mo and Cl of Hanson, Lea, Herman & Skillman (1964) and for neutral carbon from *International Tables for X-ray Crystallography* (1962). Allowance for anomalous dispersion was made only in the case of Mo radiation, using the angular independent values $\Delta f'_{Mo} = -1{\cdot}58$, $\Delta f''_{Mo} = 0{\cdot}68$, $\Delta f'_{Cl} = -0{\cdot}18$, $\Delta f''_{Cl} = 0{\cdot}163$, $\Delta f'_{C} = 0{\cdot}005$ and $\Delta f''_{C} = 0{\cdot}002$ given by Wagenfeld & Guttmann (1966). A 'unit cell' was assumed which contained 40 carbon atoms and thus had an area of 26·25 Å^2 on the basal plane. A consideration of the ratio of this area to that of the dimer phase unit cell found by electron diffraction gave a fraction of 0·97 $MoCl_5$ units per 40 carbon atoms for fully packed reactant layer. During difference Fourier refinements the parameters varied, using programs written by the author for a CDC 3200 machine, included a scale factor, one positional and thermal vibration parameter for the chlorine and two carbon layers, an occupation parameter *p* for the chlorine and molybdenum layers and a thermal parameter for the molybdenum layer. Table 6 lists the final values of these parameters for both radiations, the discrepancy index *R*, as defined previously, being 3·4% for Cu and 4·2% for Mo radiation respectively.

The interplanar spacings derived from Table 6 and listed in Table 7 differ for the two experiments but it is doubtful if this is significant, the ratio of the number of reflexions to the number of adjustable parameters being too small for the attainment of high precision. The absorption corrections, apparent low thermal parameters and lack of dispersion corrections make the Cu $K\alpha$ results less reliable than those obtained from the experiment with Mo $K\alpha$ radiation, to which the foregoing criticisms do not apply.

The small number of reflexions makes the use of normal statistical methods of error determination unwise. Consequently it is difficult to give any accurate measure of error apart from the fact that in both experiments the residual differences between F_o and F_c were equal to, or less than, the standard deviations in F_o as determined from at least three independent measurements of each reflexion. These standard deviations ranged from 2% for the strong reflexions to 20% for the weakest.

Table 5. *Final observed and calculated X-ray structure factors for 00l refinement*

			Crystal *A* Cu radiation		Crystal *B* Mo radiation	
h	k	l	F_o	F_c	F_o	F_c
0	0	1	12.3	16.9	-	5.3
		2	26.1	25.5	25.7	17.6
		3	39.2	38.8	39.2	35.3
		4	58.9	59.6	58.9	58.6
		5	102.7	109.8	101.9	104.7
		6	183.4	-183.5	183.0	-182.1
		7	<5.4	-2.7	<12.5	2.2
		8	17.3	15.9	14.3	14.7
		9	19.7	19.4	15.9	12.9
		10	13.9	9.3	<7.6	0.3
		11	55.0	-51.4	48.8	-51.9
		12	122.7	121.0	109.8	110.9
		13	55.4	57.2	40.3	43.1
		14	39.6	39.6	30.0	30.0
		15	28.5	28.5	24.4	24.3
		16	24.3	26.4	24.7	26.4
		17	90.0	86.9	71.9	75.6
		18	26.1	-25.8	23.9	-25.8
		19	<11.2	-9.1	<6.4	-3.6
		20	<11.2	-1.2	<6.1	2.4
		21	<11.1	8.1	<6.9	6.7
		22	15.1	16.0	8.7	8.4
		23	49.6*	-49.7	42.8	-41.6
		24	24.9	24.6	20.0	21.8
		25			15.6	14.8
		26			11.6	11.0
		27			<8.2	6.0
		28			<8.5	-2.0
		29			35.8	39.7
		30			<9.0	2.3

* Corrected for coincident graphite 008 reflexion.

Table 6. *Atom layer parameters derived from X-ray 00l data*

Atom layer	Crystal *A*, Cu $K\alpha$			Crystal *B*, Mo $K\alpha$			*z* if graphite spacing
	p	B_z	*z*	*p*	B_z	*z*	
C(2)	—	0·62	0·4131	—	1·17	0·4135	0·4134
C(1)	—	0·62	0·2390	—	1·3	0·2403	0·2403
Cl	0·97	1·7	0·0708	0·906	2·2	0·0697	—
Mo	0·95	1·2	0·0	0·845	1·5	0·0	—

Table 7. *Interlayer distances in* 24·8% $MoCl_5$–*graphite, free graphite and* $MoCl_5$

	Cu $K\alpha$	Mo $K\alpha$	Non-intercalated
C(2)–C(2)*	3·367 Å	3·351 Å	3·3540 ± 0·0005 Å (Bacon, 1951)
C(1)–C(2)	3·372	3·355	3·355 ± 0·001 (present work)
C(1)–Cl	3·258	3·305	—
Mo–Cl	1·371	1·350	1·32 ± 0·03†

* Across a centre of symmetry.
† Averaged value from Sands & Zalkin (1959).

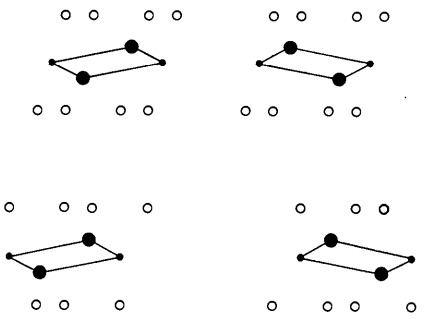

Fig. 9. Four possible positions of the dimer molecule in 24·8 % $MoCl_5$–graphite. Projection along graphite (100) planes. *c* axis compressed. Carbon atoms: open circles; Mo atoms: small spots; bridge chlorine atoms: large spots.

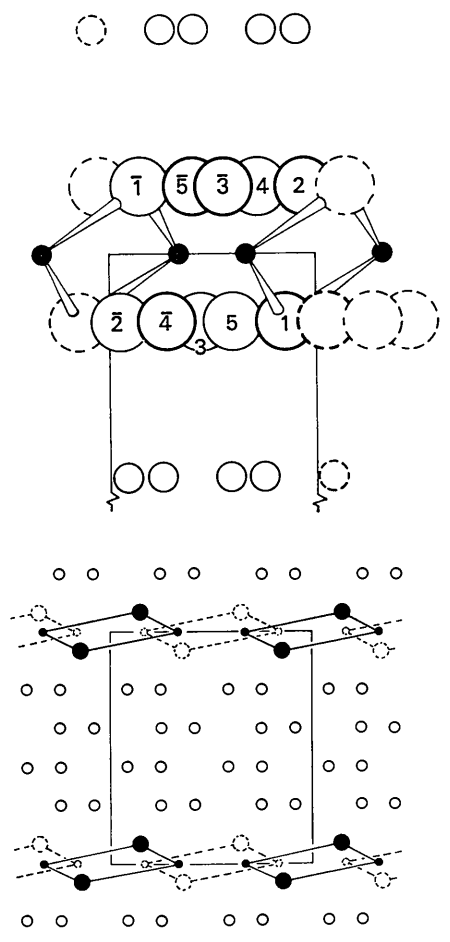

Fig. 10. The projection of the dimer phase of 24·8 % $MoCl_5$–graphite along the graphite (100) planes. Upper diagram: dimensionally correct showing all chlorine atoms, bridge bonds within the dimer molecule and the two adjacent planes of carbon atoms (small circles). Lower diagram: compressed view of upper diagram showing only those Cl atoms which are bridge bonded and alternative positions (dotted outline) for the dimer molecules. Knowledge of the horizontal position of the reactant layer relative to the graphite lattice could not be obtained in the present work and in this respect these diagrams are only illustrative.

It may be concluded with reasonable certainty that the average interlayer carbon spacing remains, independent of intercalation, within 0·05 Å of the graphite value. In addition the average Cl–C distance is a normal van der Waals contact.

hkl reflexions

The electron diffraction evidence for an exact fit of dimer phase reactant on the graphite (100) planes suggested that the two lattices would diffract coherently when the scattering vector lay in the reciprocal lattice plane containing the reactant $[2\bar{6}0]^*$, graphite $[100]^*$ and **c*** directions. Weissenberg photographs recorded with Cu $K\alpha$ radiation from crystal *B* rotated about the graphite [010] direction confirmed this suggestion. The resulting zero level record of the reflexions $h, \bar{3}h, l$ using the dimer phase indices for *h* and *k* is shown in Fig. 8. From this the *c* axis was deduced to be normal to the *ab* plane to within $\pm 2°$ and the spacing of diffuse $2h, \bar{6}h, l$ reflexions indicated the absence of glide or screw symmetry operators parallel to **c**, thus confirming the 19·37 Å identity period found previously to be the true *c* axis.

An interpretation of the *hkl* reflexions in Fig. 8 was made by a consideration of the projections of possible structures along the graphite (100) planes within the limitations of structural knowledge set by the *hk*0 and 00*l* data. In constructing these projections it was assumed that the normal $\frac{1}{3}$, $\frac{1}{3}$ interlayer translations of unintercalated graphite were maintained, that only *ABAB* or *ABCA* stacking of each set of four adjacent carbon planes was possible and that the projections were centrosymmetric. These limits reduced the number of possible positions for the dimer molecules to the four shown in Fig. 9 for the *ABAB* case.

It can be seen in Fig. 10 that the horizontal repeat distance of the reactant layer in the projection being considered is double that of the graphite. A possibility for disorder thus exists as only the very weak reactant–reactant interlayer forces can be effective in preventing mistakes of one half of the horizontal repeat distance in the stacking of reactant layers. This situation parallels that observed in wollastonite, $CaSiO_3$, by Jeffery (1953). The continuous streaks in the positions of the $1\bar{3}l$ and $3\bar{9}l$ reflexions on Fig. 8 showed this situation to exist in crystal *B*, the occupation of the full and dotted line reactant sites in Fig. 10 having equal probability. The calculations of structure amplitudes were therefore based on an average cell which was half that shown in the lower half of Fig. 10. However, before proceeding it was necessary to reconcile the symmetry of the trial structures, always no greater than *p*2, independent of the reactant, with the observed symmetry. Plane group *p*2 requires $F_{(h,\bar{3}h,l)} \neq F_{(\bar{h},3h,l)}$, but the observed intensities of these reflexions were equal. An explanation lies in the mechanism of the intercalation process. This will start independently at many sufficiently widely spaced points on the prismatic faces of

a graphite crystal. Consequently penetrations at zig and zag positions, as shown in Fig. 11, are equally probable, giving rise to twinning on the graphite (100) plane, the twin axis being arrowed in Fig. 11. As a result the calculated numbers $\bar{F}_c$ compared with the observed amplitudes were derived from the relation

$$\bar{F}_c=(F^2_{h'0l}+F^2_{\bar{h}'0l})^{\frac{1}{2}}$$

where $F_{h'0l}$ is the normal structure amplitude with indices referred to the average unit cell outlined in Fig. 10.

Table 8 shows the results of the first calculations in which only carbon atom contributions were included. Of the two stacking possibilities *ABCA* and *ABAB*, the *R* index was 58% for the former and 20% for the latter. Inclusion of varying amounts of reactant in any of the four positions shown in Fig. 9 with the *ABAB* carbon model did not change any signs of the $F_{h'0l}$ or reduce *R* below 20%. This can be readily understood when the lateral rigidity of the graphite lattice is considered, as it necessitates only a few widely spaced islands of correctly oriented reactant to bind the carbon layers into a coherently diffracting crystal.*

Electron microscope observations

To ascertain the microscopic nature of the intercalated graphite and confirm the structural conclusions drawn from diffraction evidence concerning the dimer phase, dark-field images were obtained from both the graphite and $MoCl_5$ layers of a thin intercalated crystal. The work was done with an HU 11-A microscope using tilted illumination and a magnification of 10000.

Accurate diffraction pattern measurements showed that the departure of the true reactant unit cell from sixfold point symmetry should lead to the appearance of Moiré fringes of approximately 200 Å spacing in the dark-field images of two overlapping, dimer reactant layers of differing orientation. Further, any deviations from perfection in the layers will be revealed by distortions of the Moiré fringes.

When the 0,10; 3,5; $3,\bar{5}$ reflexion is used interference will occur between the 0,10 beam of one layer and either the 3,5 or $3,\bar{5}$ beam of the other. Fig. 12 shows fringes occurring at *A* where two differently oriented rafts of reactant, whose outlines may be clearly seen, overlap. At *B* a third orientation causes a rapid modulation of the fringes, a variation of the general case (*C*) in which three fringes sets at angles of approximately 60° appear. Phase changes between superimposed rafts having the same orientation will result in the intensity variations seen at *D*, in the Moiré fringes at *A*, and elsewhere. The position, varied spacing and distortion of the fringes strongly supports the diffraction evidence for a small, irregular location of the dimer molecules along their orienting graphite (100) planes and the incomplete nature of intercalation.

No systematic study of dislocations in graphite and their modification by intercalation was conducted as these problems have been treated by Amelinckx & Delavignette (1960, 1961), Heershcap, Delavignette & Amelinckx (1964), and Eeles & Turnbull (1965). Graphite 100 dark field images, from 24·8% $MoCl_5$–graphite, as seen in Fig. 13, show general features such as individual dislocation lines at *E*, similar to those of other workers. There was no correspondence between any features in dimer phase reactant images and those in the graphite images apart from one exception. This occurs at *F* in Fig. 13, where Moiré fringes surround a flat topped protrusion from the graphite crystal.

Table 8. *The observed and calculated amplitudes averaged over twin orientations for the* $h,\bar{3}h,l$ *reflexions of* 24·8% $MoCl_5$–*graphite. Carbon contributions only*

The indices refer to the unit cell outlined in Fig. 10

	ABAB		*ABCA*	
h'kl	F_o	F_c	F_o	F_c
200 }	35 37	{ 32	30 27	{ 16
1 }		{ 18		{ 21
2	35	30	30	45
3	66	52	58	27
4	<6	15	<5	42
5	22	22	19	10
6	25	26	22	12
7	11	7	9	25
8	27	30	23	30
9	35	34	30	23
10	<9	2	<8	26
11	11	17	9	6
12	11	16	9	5
13	<11	2	<9	21
14	19	24	16	17
15	16	19	13	19
400	24	15	23	8
1	21*	9	20*	10
2	14*	14	14*	22
3	35	26	34	13
4	<12	8	<12	21
5	12	11	12	5
6	16	14	15	6
7	<12	4	<12	14
8	16	17	15	18
9	23	21	22	14

* Overlapped reflexions, approximate ratio.

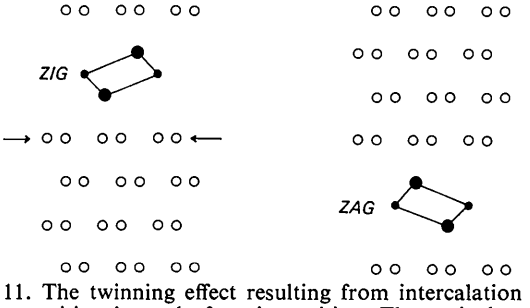

Fig. 11. The twinning effect resulting from intercalation at a zag position instead of a zig position. The equivalent twin axis (arrowed) is in the plane of the paper.

* If all reactant in 35·5% $MoCl_5$–graphite was in the dimer phase, one-third contributing to the particular $h,\bar{3}h,l$ pattern being examined, the reactant would contribute roughly one-sixth of the scattered intensity.

Dark-field reactant images from the three dimer orientations other than those contributing to Fig. 12 showed the protrusion to contain reactant. Rough estimates of the minimum height of the protrusion made by counting the surrounding fringes gave a result of 50 Å. Other protrusions of greater size and height were frequently observed, particularly if a high electron beam current was used. They were characterized by curved tops and did not contain reactant that diffracted strongly in the direction of the 0,10; 3,5; 3,$\bar{5}$ reflexions.

Discussion

A significant result of the present study is the observation of a precise lateral, one-dimensional fit of the dimer reactant phase and the graphite. Since a small distortion of the reactant structure is required in order to achieve this fit, there must exist a particularly favourable juxtaposition (in one dimension) of reactant and carbon atoms. It can be seen in the projection of Fig. 10 that no obvious special relations exist between adjacent carbon and chlorine atoms. However, the Mo–Mo distances are an exact multiple of the distance between carbon atoms. This fact supports the theory of bonding in metal-halide–graphite compounds put forward by Croft (1956*b*) which requires the transfer of conduction band electrons from graphite to the cation. The non-observation of a similar carbon–cation juxtapositioning in the case of hexagonal reactant phases presumably results from the infinite two-dimensional nature of the reactant molecule. Consequently, the most vivid exposure of the effects of reactant–carbon forces on the structure may be expected in compounds having finite reactant molecules.

An important feature of the electron diffraction patterns is the diffuse arcs which join the dimer phase 0,10; 3,5; 3,$\bar{5}$ reflexions to the 30 reflexions of the 3·7° hexagonal phase. In addition similar, weaker arcs are observed joining all hexagonal phase reflexions receiving chlorine scattering contributions to the corresponding reflexions of the dimer phase. The bowed-in arcs visible in Fig. 1 lying across the graphite [110]* direction between adjacent 30 (hex.) reflexions were not typical; generally only those directed to the nearest dimer reflexion were present. The chlorine atoms contributing to these arcs are in the process of reorienting themselves as ordering of cations into dimer pairs occurs. The unfavoured transition between adjacent 3·7° hexagonal phases is accompanied by an increase in the mean Cl–Cl distance parallel to the layer plane.

The author is indebted to the Division of Chemical Physics, C.S.I.R.O. and the University of Western Australia for providing facilities without which the present work would not have been possible. It is a pleasure to acknowledge the assistance and stimulating discussion of Mr A. F. Moodie.

References

AMELINCKX, S. & DELAVIGNETTE, P. (1960). *J. Appl. Phys.* **31**, 2126.
AMELINCKX, S. & DELAVIGNETTE, P. (1961). *Direct Observation of Imperfections in Crystals*, p. 295. New York: Interscience Publishers.
BACON, G. E. (1951). *Acta Cryst.* **4**, 558.
BADER, R. F. W. & WESTLAND, A. D. (1961). *Canad. J. Chem.* **39**, 2307.
COLTON, R. & TOMKINS, I. B. (1964). *Aust. J. Chem.* **18**, 447.
COWLEY, J. M. & IBERS, J. A. (1956). *Acta Cryst.* **9**, 421.
CROFT, R. C. (1956*a*). *Aust. J. Chem.* **9**, 184.
CROFT, R. C. (1956*b*). *Aust. J. Chem.* **9**, 194.
CROFT, R. C. (1960). *Quart. Rev. Chem. Soc. Lond.* **14**, 1.
DAWSON, B. (1961). *Acta Cryst.* **14**, 1120.
EELES, W. T. & TURNBULL, J. A. (1965). *Proc. Roy. Soc.* **283** A, 179.
FUJIWARA, K. (1961). *J. Phys. Soc. Japan*, **16**, 2226.
GOODMAN, P. & LEHMPFUHL, G. (1967). *Acta Cryst.* **22**, 14.
HANSON, H. P., LEA, J. D., HERMAN, F. & SKILLMAN, S. (1964). *Acta Cryst.* **17**, 1040.
HEERSHCAP, M., DELAVIGNETTE, P. & AMELINCKX, S. (1964). *Carbon*, **1**, 235.
HENNIG, G. R. (1959). *Progr. Inorg. Chem.* **1**, 125.
International Tables for X-ray Crystallography (1962). Vol. III. Birmingham: Kynoch Press.
JEFFERY, J. W. (1953). *Acta Cryst.* **6**, 821.
PARRISH, W. (1960). *Acta Cryst.* **13**, 838.
REICHE, W. D. (1961). *Optik*, **18**, 278.
RÜDORFF, W. (1959). *Advanc. Inorg. Radiochem.* **1**, 223.
RÜDORFF, W., STUMPP, E., SPRIESSLER, W. & SIECKE, F. W. (1963). *Angew. Chem.* **75**, 130.
SAEKI, Y. & MATSUZAKI, R. (1965). *Denki Kagaku*, **33**, 155.
SANDS, D. E. & ZALKIN, A. (1959). *Acta Cryst.* **12**, 723.
UBBELOHDE, A. R. & LEWIS, F. A. (1960). *Graphite and its Crystal Compounds*, p. 132. Oxford: Clarendon Press.
WAGENFELD, H. & GUTTMANN, A. J. (1966). Private communication.